LETTER • OPEN ACCESS

Improving inverse Compton sources by avoiding non-linearities

Improving inverse Compton sources by avoiding non-linearities

B. Terzić[1] , G. A. Krafft[1,2], V. Petrillo[3,4], I. Drebot[3] and M. Ruijter[3,5]

[1] *Department of Physics, Center for Accelerator Science, Old Dominion University - Norfolk, VA 23529, USA*
[2] *Thomas Jefferson National Accelerator Facility - Newport News, VA 23606, USA*
[3] *INFN-Milan - via Celoria 16, 20133 Milano, Italy*
[4] *Università degli Studi di Milano - via Celoria 16, 20133 Milano, Italy*
[5] *Università di Roma La Sapienza - P. le A. Moro 5, 00185 Roma, Italy*

Abstract – We present a new, more nuanced understanding of non-linear effects in inverse Compton sources. Deleterious non-linear effects can arise even at low laser intensities, a regime previously viewed as linear. After laying out a survey of non-linear phenomena which degrade the effectiveness of inverse Compton sources, we discuss two powerful techniques designed to avoid these non-linearities. Starting with the known technique of non-linear longitudinal chirping of the laser pulse in the high laser field regime, we show that the simple stretching of the laser pulse, while keeping the energy constant, can significantly increase the spectral density of the scattered radiation in many operating regimes. Our numerical simulations show that combining these two techniques avoids detrimental non-linearities and improves the performance of inverse Compton sources over an order of magnitude.

Introduction. – X-rays enable scientists to see the internal structure of materials on all length scales from the macroscopic down to the positions of individual atoms. This capability has had profound impact on science, technology, and on the world economy. It is impossible to overstate this impact, from Nobel Prize winning science to the everyday dental x-ray. The science and technology community agrees that future advances in many areas depend on understanding structure/function relationships at the nano-scale where new properties emerge, and controlling the fabrication of complex materials at that scale to achieve transformative physical, chemical, and biological functionality.

The sources of x-ray radiation relying upon Compton scattering [1,2] possess a notable advantage over the traditional bremsstrahlung sources —the narrow-band nature of the radiation emerging from them, allowing particularly large values of the spectral density. This motivated creation of designated facilities featuring inverse Compton sources (ICS) [3], which have been applied to x-ray structure determination [4], dark-field imaging [5,6], phase contrast imaging [5], and computed tomography [7].

As a significantly more affordable alternative to large facility sources, inverse Compton sources of x-rays may allow a multitude of studies not easily accomplished at the large facilities. These potentially groundbreaking studies in medicine, pharmaceutical industry, chemistry, material science, homeland security and many other fields of human endeavor, hold a promise of fundamentally improving our lives.

Operating or projected ICS can be conceived following various paradigms: a first class of infrastructures [5,7–9] is based on laser pulses produced in cavities and electron beams accelerated in storage rings or in Energy Recovery Linacs, with shots producing a low number of photons (10^3–10^5 photons/shot), reiterated at high repetition rate (100 MHz class). In these facilities, the interaction is always linear, because the laser field strength parameter turns out to be $a_0 \ll 1$. A different concept of ICS, instead, is based on electron beams accelerated in warm linacs [10–16] or in plasma accelerating stages [17,18], operating at low repetition rate (1–120 Hz), colliding with
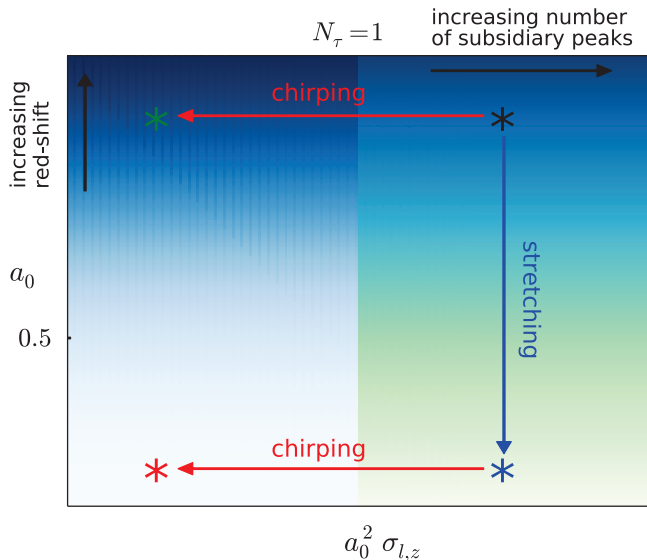
Fig. 1: Regimes of operation of ICS, as listed in table 1. Blue line pointing downward represents stretching the laser pulse (increasing its length $\sigma_{l,z}$), while keeping the energy of the laser constant ($a_0^2 \sigma_{l,z} = $ const). Red lines pointing to the left represent chirping the laser pulse, which removes subsidiary peaks. Stars denote parameters for simulations carried out in figs. 2 and 3, each color corresponding to the spectrum of the same color.

high-energy J-class lasers. In this case, the photon number per second is accumulated by summing up the intense output (10^8–10^9 photons/shot) of few single shots, with the possibility of strong non-linear effects in the interaction.

In this letter, we map out the regimes of operations for ICS and describe the non-linear effects which plague each of these regimes. We then present two precise techniques which combine to largely remove these non-linearities, thereby substantially improving the peak spectral density of the scattered radiation emerging from these sources.

Regimes of operation of inverse Compton sources. – In ICS, a relativistic electron beam interacts with a high-field laser beam, producing intense and highly collimated electromagnetic radiation via Compton scattering [2]. Through relativistic upshifting and the relativistic Doppler effect, highly energetic polarized photons are radiated along the electron beam motion when the electrons interact with the laser light.

The strength of the laser field is quantified by the amplitude (a_0) of the normalized vector potential $\tilde{A}(\xi) = eA(\xi)/m_e c = a(\xi)\cos(2\pi\xi/\lambda)$, where $a(\xi)$ is the amplitude envelope, $\xi = z + ct$ is the coordinate along the laser pulse, λ the wavelength of the laser. At high laser field intensities, the spectrum of backscattered radiation is considerably broadened because of the changes in the longitudinal velocity of the electrons during the pulse. Such ponderomotive line broadening in the scattered radiation makes the bandwidth too large for some applications and reduces the spectral brilliance.

Table 1: Regimes of operations for ICS, as shown in fig. 1, color-coded.

Regime	$a_0^2 s$	a_0	Non-linearities
Linear (white)	$N_\tau \lesssim 1$	$a_0 \lesssim 0.5$	none
Non-linear (green)	$N_\tau \gtrsim 1$	$a_0 \lesssim 0.5$	subs. peaks
Non-linear (blue)	$N_\tau \lesssim 1$	$a_0 \gtrsim 0.5$	red-shift
Non-linear (aqua)	$N_\tau \gtrsim 1$	$a_0 \gtrsim 0.5$	red-shift, subs. peaks

The onset of non-linear ponderomotive line broadening has been associated with the increase of the laser field strength [19–21]. The two main mechanisms which bring about non-linear ponderomotive broadening of the spectra are: 1) non-linear subsidiary peaks [21–23] and 2) non-linear redshift. The interplay between the two effects is shown in fig. 1, with each axis quantifying the importance of each. The parameters for the simulations shown in the figure are given in table 1.

Non-linear subsidiary peaks and their removal. – The linear spectrum features solitary, narrow peaks. One of the signatures of spectral non-linearities is the appearance of multiple peaks around each harmonic. These non-linear subsidiary peaks in the scattered spectra at high laser intensities have been predicted and their number empirically approximated for a gaussian laser envelope and $\lambda = 80$ nm in refs. [24,25]. The exact number of subsidiary peaks for an arbitrary laser envelope and wavelength was derived in ref. [20]. For the Gaussian envelope we consider here, it is

$$N_\tau = \frac{\sqrt{\pi}}{2} a_0^2 \frac{\sigma_{l,z}}{\lambda}, \tag{1}$$

where $\sigma_{l,z}$ is the physical length of the laser pulse. For $N_\tau > 1$, additional peaks appear in the spectrum, thereby reducing the spectral density in the primary peak. In experiments so far, subsidiary peaks have not been definitively observed because of the dominant broadening effect of the electron beam energy spread and emittance. A trace of them has been observed in ref. [23].

From eq. (1), it follows that the number of subsidiary peaks does not depend on the strength of the laser field a_0 alone, but on the combination of the strength of the laser field and the length of the laser, $a_0^2 \sigma_{l,z}$. This means that it is possible for a spectrum to feature non-linear subsidiary peaks even at low a_0, a regime previously viewed as linear, if the laser is long enough. The spectrum shown in blue in the middle panel of fig. 2, which represents $a_0 = 0.1$, is an illustration of such case.

Removing subsidiary peaks and restoring the narrow-band nature of the spectrum is accomplished by exact laser chirping, which changes the normalized vector potential to $\tilde{A}(\xi) = a(\xi)\cos(2\pi\xi f(\xi)/\lambda)$, where $f(\xi)$ is the chirping prescription [20]:

$$f(\xi; a_0) = \frac{1}{1 + a_0^2/2} \left(1 + \frac{1}{2\xi}\int_0^\xi a^2(\xi')\mathrm{d}\xi'\right). \tag{2}$$
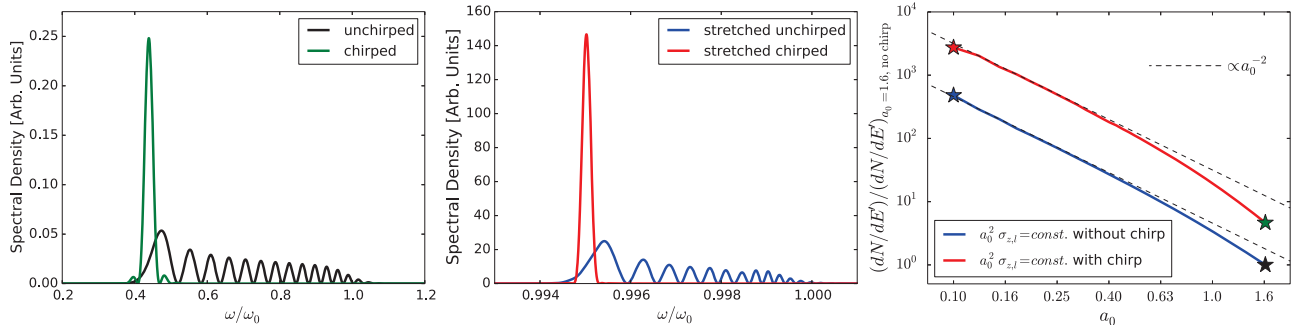
Fig. 2: Backscattered spectra for a single, on-axis 45 MeV electron colliding with a 1D plane wave laser with wavelength of $\lambda = 800$ nm. Left and middle panels use the same arbitrary units. Left panel: an unchirped (black line) and chirped (green line) laser with $a_0 = 1.6$, $\sigma_{l,z} = 4.46\,\mu$m. Chirping increases the peak spectral density by 4.6 times. Middle panel: an unchirped (blue line) and chirped (red line) laser with $a_0 = 0.1$, $\sigma_{l,z} = 1.14$ mm. Chirping increases the peak spectral density by 5.3 times. Stretching increases the peak spectral density by 480 times (unchirped laser) and 591 times (chirped laser). Combined, stretching and chirping increase the spectral density by 2738 times. Right panel: The relative increase in peak spectral density, normalized to the spectral density of the unchirped case at $a_0 = 1.6$, as a function of the laser field strength parameter a_0.

Exact laser chirping was shown to be perfectly effective for restoring narrow-band property of the back-scattered radiation produced in scattering a 1D plane wave laser with an on-axis, single-electron, without [20,26–28] and with radiation reaction [29]. Laser chirping remains effective even for electron beams with moderate energy spread [30]. It has been shown, however, that the perfect compensation removes the ponderomotive broadening completely for just a single scattering angle for all harmonics. For all other angles, the ponderomotive broadening is not completely compensated [27]. Improving the laser model to a 3D laser pulse brought about a generalized chirping prescription when colliding with a single on-axis electron [31], which, while not perfect, is still quite effective. Finally, in the realistic scenario of a collision between a 3D laser pulse and a general electron beam distribution, we have shown that the optimal form of laser chirping can be found using an optimization over the parameters of the chirping prescription [19]. The effectiveness of such chirping depends on the relative transverse sizes of the two colliding beams and can still be quite effective when the transverse size of the laser pulse is roughly the size of the electron beam or larger [19].

Therefore, laser chirping removes subsidiary peaks, leaving only one dominant peak per harmonic. The effect of laser chirping on the landscape of regimes of operation for ICS shown in fig. 1 is to move horizontally from the region where $N_\tau \gg 1$ to the region where $N_\tau \approx 1$.

Non-linear red-shift and its removal. – The linear spectrum contains a dominant, narrow peak centered around the frequency $\omega_0 = (1 + \beta)^2 \gamma^2 2\pi c/\lambda$. However, as the magnitude of the normalized vector potential a_0 grows, the peak experiences non-linear red-shift:

$$\omega = \frac{\omega_0}{1 + a_0^2/2}. \tag{3}$$

The non-linear shift is accompanied by widening of the peaks. This is evident from the comparison of the location of the primary harmonic in spectra in the left and middle panel of fig. 2.

From the eq. (3), it is clear that the non-linear shift will be reduced if a_0 is reduced. If the total energy in the laser pulse is kept constant, the reduction in a_0 can only come at an appropriate increase in the laser volume V, because the laser intensity I is given by

$$I = \frac{cE}{V} = \frac{2\pi^2 m_e^2 c^3}{\lambda^2 e^2 \mu_0} a_0^2, \tag{4}$$

where E is the laser energy

$$E = \frac{2\pi^2 m_e^2 c^2}{\lambda^2 e^2 \mu_0} a_0^2 V. \tag{5}$$

For a Gaussian laser pulse, both transversally and longitudinally, $V = (2\pi)^{3/2} \sigma_{l,x} \sigma_{l,x} \sigma_{l,z}$, where $\sigma_{l,x}$ is the horizontal and $\sigma_{l,y}$ vertical size of the laser pulse, m_e is the mass of the electron, c is the speed of light e is the elementary charge and μ_0 is the permeability of vacuum. Therefore, to keep the energy constant, reducing a_0 must be done in such a manner that the quantity $a_0^2 V$ is kept constant. This means that reducing a_0 by some factor is accomplished by making the volume (the transverse or longitudinal size, or a combination thereof) larger by a square of that factor. In the case of the 1D laser pulse model, the only way to increase the volume of the laser is by stretching it (increasing its longitudinal size). In the case of a 3D laser pulse model, the increase in volume can be done by either stretching the beam or increasing its cross-section (transverse size). However, increasing the cross-section of the laser while keeping the energy constant will result in the net reduction of peak spectral density. While increasing the transverse size of the laser pulse leads to a more favorable distribution of effective laser field strength parameter a_0 that electrons experience [19], the peak spectral density will be dominated by its dependence on $a_0^2 \sigma_{l,z}^2$ [30].

This realization suggests a simple method of reducing the deleterious effects of non-linear red-shift: stretching

the laser beam while keeping its energy constant. The effects of this approach on peak spectral density are presented next, first for the 1D plane wave and then for the 3D pulse laser model.

Spectra from a single, on-axis electron scattering. – We verify these ideas through numerical simulations. The theory and the code for an on-axis, single-electron collision with a 1D laser pulse was developed in ref. [21]. In ref. [20], we generalized the theory and the code to model an arbitrary laser chirp. The code has been further improved to carry out simulations for electron beams with energy spread [30]. Finally, we recently developed another code, still based on the original theory developed for a single-electron scattering off a 1D (chirped or unchirped) laser pulse [20,21], to model scattering of a 3D (chirped or unchirped) laser pulse off a realistic electron beam (with emittances and energy spread). This is the most general code, named SENSE (Simulation of Emitted Non-linear Scattering Events), subsuming all previous versions. It is described in detail in ref. [19]. It is valid in a regime where electron recoil can be neglected, or, in terms of the subsidiary peaks, $N_\tau \leq 3/(4\alpha) \approx 103$, where α is the fine structure constant. This is not a very restrictive range, because most of the existing and future ICS are situated comfortably within this regime. SENSE can be used to compute a spectrum from a single, on-axis electron scattering off a 1D plane wave (using a 3D model in the 1D limit $\sigma_{l,x}, \sigma_{l,y} \gg \sigma_{l,z}$). We can also use it for fully realistic simulations —including electron beams with energy spread and emittance and a 3D laser pulse with the finite transverse extent— of an existing ICS.

The individual effects of stretching of the laser and chirping are best visualized separately. We do that by following the path marked by the colored stars in fig. 1. We start with an unchirped case with high a_0 (the black star in fig. 1 and the black line in the left panel of fig. 2) and stretch the laser pulse to the unchirped case with a low a_0 (the blue star in fig. 1 and the blue line in the middle panel of fig. 2), shown in the left panel of fig. 2. We then chirp the laser for both the low-a_0 (the red star in fig. 1 and the red line in the middle panel of fig. 2), and the high-a_0 case (the green star in fig. 1 and the green line in the left panel of fig. 2), shown in the middle panel of fig. 2.

While at constant energy ($a_0^2 \sigma_{l,z} = $ const; moving vertically in fig. 1), the spectra look similar in shape when scaled by the non-linear offset $1/(1 + a_0^2/2)$. In the low-a_0 regime, the height of the peak is directly proportional to $a_0^2 \sigma_{l,z}^2$ [30]:

$$\frac{\mathrm{d}^2 E}{\mathrm{d}E'\mathrm{d}\Omega} = \frac{\pi\alpha}{2}\gamma^2(1+\beta)^2 a_0^2 \frac{\sigma_{l,z}^2}{\lambda^2}, \qquad (6)$$

where it is assumed that the collecting aperture is small enough that the spread it generates is less then the spread from the pulse and the spectral height is less than the pedestal level [32]. Therefore, at constant $a_0^2 \sigma_{l,z}$, the peak

spectral density scales as a_0^{-2}. This dependence is verified in simulations for $a_0 \lesssim 0.5$, carried out for the fixed laser energy ($a_0^2 \sigma_{l,z} = $ const) and is shown in the right panel of fig. 2, for both unchirped and chirped lasers. For $a_0 \gtrsim 0.5$, the drop in peak spectral density with increasing a_0 is even more precipitous because of 1) the relative importance of the higher-order harmonics increases with a_0, from being negligible at $a_0 \lesssim 0.5$ to rivaling the primary harmonic at $a_0 \gtrsim 1$ [30]; and 2) the complete merger of all harmonics at $a_0 \gtrsim 2$.

Spectra from an electron beam scattering. – Taking a couple of steps forward in terms fidelity of computational modeling to the physical problem, we carry out numerical simulations with SENSE for a collision of an electron beam —specified by its bulk properties of emittance, size and energy spread— and a 3D laser pulse. We use parameters from an actual experiment, and simulate what would happen if the laser in the experiment was changed —stretched and/or chirped. Chirping is implemented by varying a_0 in eq. (2).

We choose to model a recent experiment at the ICS in Dresden, reported in ref. [33], which we recently simulated in detail [19]. In our simulation, the electron beam is kept constant, possessing the same properties as the electron beam in the Dresden experiment [33]: 45 MeV mean energy, energy spread of 0.00175, with normalized emittances $\epsilon_{x,n} = 20.3$ mm mrad, $\epsilon_{x,n} = 18$ mm mrad, longitudinal size $\sigma_z = 1.1$ mm, transverse size $\sigma_x = 41\,\mu$m, $\sigma_y = 81\,\mu$m. The laser parameters are: wavelength $\lambda = 800$ nm, pulse duration $T = 14.86$ fs, transverse size $\sigma_{l,x} = \sigma_{l,y} = 13.59\,\mu$m. The experimental results for four different values of the laser field strength a_0 were reported in the paper [33]: 1.6, 1.0, 0.5 and 0.05. Here we focus on $a_0 = 1.6$, because in this case the non-linearities are most pronounced.

Again, we visualize the individual effects of stretching of the laser and chirping separately by following the path marked by the colored stars in fig. 1. We start with an unchirped case with high a_0 (the black star in fig. 1 and the black line in the left panel of fig. 3) and stretch the laser pulse to the unchirped case with a low a_0 (the blue star in fig. 1 and the blue line in the middle panel of fig. 3), shown in the left panel of fig. 3. We then chirp the laser for both the low-a_0 (the red star in fig. 1 and the red line in the middle panel of fig. 3), and the high-a_0 case (the green star in fig. 1 and the green line in the left panel of fig. 3), shown in the middle panel of fig. 3.

The improvements in the peak spectral density due to chirping are considerably more modest for scattering off an electron beam than in the case of a single, on-axis electron. As the electrons from a beam collide with a laser pulse, they will experience a wide range of laser field strength parameters a_0 [19]. Exact chirping prescription in eq. (2) depends on a_0, and can perfectly compensate the nonlinearities in the spectrum only for electrons experiencing
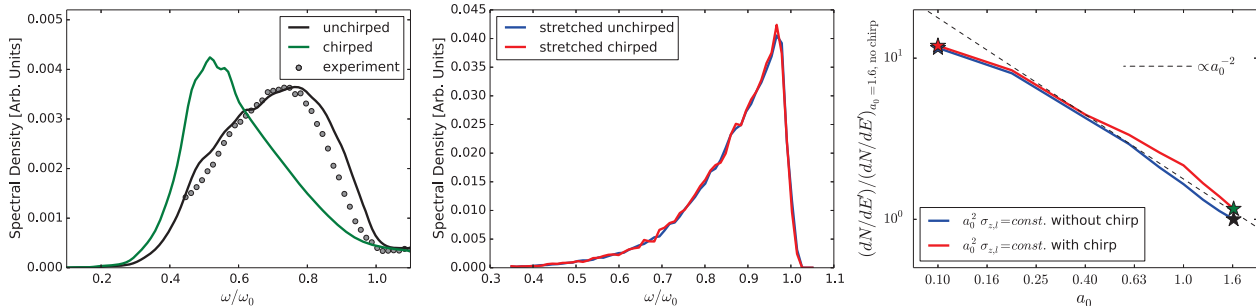
Fig. 3: Spectra for a scattering event as for $a_0 = 1.6$ in ref. [32]: 45 MeV electron beam with normalized transverse emittances $\epsilon_{x,n} = 20.3$ mm mrad, $\epsilon_{x,n} = 18$ mm mrad, transverse size $\sigma_x = 41\,\mu m$, $\sigma_y = 81\,\mu m$, and the energy spread of 0.00175, colliding with a 3D plane wave laser with wavelength of $\lambda = 800$ nm and transverse size $\sigma_{l,x} = \sigma_{l,y} = 13.59\,\mu m$. The maximum aperture is $\theta_a = 0.004$ backscattered along the collision axis. Left and middle panels use the same arbitrary units. Left panel: an unchirped (black line) and chirped (green line) laser with $a_0 = 1.6$ and $\sigma_{l,z} = 4.46\,\mu m$; experimental data from ref. [33] (grey points). Chirping increases the peak spectral density by 16%. Middle panel: The laser pulse is stretched longitudinally so as to keep $a_0^2\sigma_{l,z} = $ const: an unchirped (blue line) and chirped (red line) laser with $a_0 = 0.1$ (blue line) and $\sigma_{l,z} = 1.14$ mm. Chirping is not effective. Stretching increases the peak spectral density by about 12 times for both unchirped and chirped lasers. Right panel: The relative increase in peak spectral density, normalized to the spectral density of the unchirped case at $a_0 = 1.6$, as a function of the laser field strength parameter a_0.
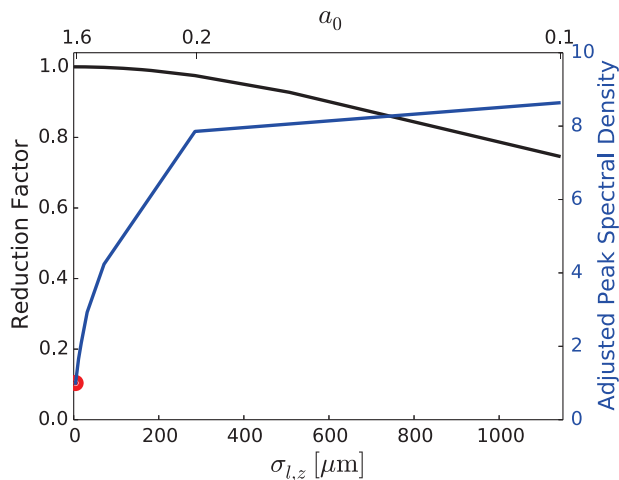

Fig. 4: Reduction in the total number of scattered photons due to hourglass effect (black line), normalized to the value at nominal parameters $a_0 = 1.6$ and $\sigma_{l,z} = 4.46\,\mu m$. Blue line shows the peak spectral density of a stretched beam in the Dresden experiment (nominal parameters of the experiment are denoted by a red circle), adjusted for the hourglass effects (to be compared to the unadjusted blue line in the right panel of fig. 3).

one value of the laser field strength. Therefore, the majority of the electron distribution does not see the perfect chirping prescription.

As the laser field strength a_0 reduces while keeping the energy constant, the longitudinal size of the laser $\sigma_{l,z}$ increases, and the energy spread of the pulse decreases. Stretching the laser pulse reduces its energy spread —in both chirped and unchirped case— and its contribution to the scattered linewidth becomes negligible when compared to the other sources, such as electron beam emittance. This is indeed observed from the middle panel of fig. 3: a spectrum is dominated by electron beam emittance, while

chirping is not effective. A comprehensive discussion of the scaling laws in ICS is presented in refs. [32,34–36], along with clear illustrations of what spectra dominated by various sources of linewidth look like. The asymmetry and the hard high-energy edge in the spectrum in the middle panel of fig. 3 are clear signs of dominanice of electron beam emmitance.

In ref. [19], we demonstrate that the effectiveness of chirping in improving the peak spectral density becomes more pronounced as the electron beam emittance is reduced. This is to be expected, since reducing the beam emittance reduces its size relative to that of the laser pulse, thereby approaching the 1D plane wave limit [19].

The impact of laser stretching on peak spectral density is still substantial. In the case simulated here, beam stretching from the nominal experimental setup for $a_0 = 1.6$ to $a_0 = 0.1$ increases the peak spectral density by about a factor of 10.

As the laser pulse is stretched, its three-dimensional focus geometry leads to decreasing laser intensities. This geometric reduction in scattering rates is called the hourglass effect [37]. Figure 4 shows the geometric reduction in total scattering events (black line) with respect to the nominal parameters at $a_0 = 1.6$ and $\sigma_{l,z} = 4.46\,\mu m$. For the case considered here, it is not significant —on the order of 30% at $a_0 = 0.1$. The blue line in fig. 4 shows the peak spectral density adjusted for hourglass effect.

Conclusion. – We put forward a new, more subtle, understanding of non-linearities in ICS. One novel realization is that non-linear subsidiary peaks in the scattered spectra can arise even at low values of the laser field strength parameter a_0, a region previously thought of as linear. Another new idea presented here, more profound and consequential in magnitude, is that the deleterious non-linear redshift can be removed by stretching the laser pulse while keeping its energy constant. This stretch-

ing alone improves the peak spectral density by over an order of magnitude. In the cases when the linewidth of scattered radiation is not dominated by the electron beam emittance, laser chirping can remove subsidiary peaks from individual spectra, thereby further improving the peak spectral density. Overall, combining these two approaches —stretching and chirping of the laser beam— mitigates both non-linear manifestations which are detrimental to spectral linewidth: non-linear red-shift and subsidiary peaks. This leads to substantial improvement in the performance of ICS.

The most important implication of our findings is that the ICS do not need high-field lasers to produce high-yield radiation. In fact, given the same laser energy, operating at lower field strengths increases the peak yield by a substantial factor, often exceeding an order of magnitude. This substantially reduces the challenge of designing and operating high-field lasers, thereby lowering their cost and increasing the prospect of their wide-spread availability.

$$* * *$$

REFERENCES

[1] Jackson J. D., *Classical Electrodynamics* (Wiley) 2007.
[2] Krafft G. A. and Priebe G., *Rev. Accel. Sci. Technol.*, **03** (2010) 147.
[3] Huang Z. and Ruth R. D., *Phys. Rev. Lett.*, **80** (1998) 976.
[4] Abendroth J., McCormick M. S., Edwards T. E., Staker B., Loewen R., Gifford M., Rifkin J., Mayer C., Guo W., Zhang Y., Myler P., Kelley A., Analau E., Hewitt S. N., Napuli A. J., Kuhn P., Ruth R. D. and Stewart L. J., *Phys. Rev. Accel. Beams*, **11** (2010) 91.
[5] Bech M., Bunk O., David C., Ruth R., Rifkin J., Loewen R., Feidenhans'l R. and Pfeiffer F., *J. Synchrotr. Radiat.*, **16** (2009) 43.
[6] Schleede S., Meinel F. G., Bech M., Herzen J., Achterhold K., Potdevin G., Malecki A., Adam-Neumair S., Thieme S. F., Bamberg F., Nikolaou Ko., Bohla A., Yildirim A. Ö., Loewen R., Gifford M., Ruth R., Eickelberg O., Reiser M. and Pfeiffer F., *Proc. Natl. Acad. Sci. U.S.A.*, **109** (2012) 7880.
[7] Achterhold K., Bech M., Schleede S., Potdevin G., Ruth R., Loewen R. and Pfeiffer F., *Sci. Rep.*, **3** (2013) 1313.
[8] Favier P., Amoudry L., Cassou K., Dupraz K., Martens A., Monard H. and Zomer F., *Proc. SPIE*, **10387** (2017) 1038708.
[9] Drebot I., Bacci A., Bosotti A., Broggi F., Canella F., Cardarelli P. and Cialdi S., *Instruments*, **3** (2019) 49.
[10] Pogorelsky I. V., Ben-Zvi I., Hirose T., Kashiwagi S. *et al.*, *Phys. Rev. ST Accel. Beams*, **3** (2000) 090702.
[11] Babzien M., Ben-Zvi I., Kusche K., Pavlishin I. V., Pogorelsky I. V., Siddons D. P., Yakimenko V., Cline D., Zhou F., Hirose T., Kamiya Y., Kumita T., Omori T., Urakawa J. and Yokoya K., *Phys. Rev. Lett.*, **96** (2006) 054802.
[12] Brown W., Anderson S., Barty C., Betts S., Booth R., Crane J. *et al.*, *Phys. Rev. ST Accel. Beams*, **7** (2004) 060702.
[13] Kuroda R., Toyokawa H., Yasumoto M., Ikeura-Sekiguchi H., Koike M., Yamada K., Yanagida T., Nakajyo T., Sakai F. and Mori K., *Nucl. Instrum. Methods Phys. Res. A*, **637** (2011) 183.
[14] Du Y., Yan L., Hua J., Du Q., Zhang Z., Li R., Qian H., Huang W., Chen H. and Tang C., *Rev. Sci. Instrum.*, **84** (2013) 053301.
[15] Vaccarezza C. *et al.*, *Nucl. Instrum. Methods Phys. Res. A*, **829** (2016) 237.
[16] Faillace L. *et al.*, in *Advances in Laboratory-Based X-Ray Sources, Optics, and Applications*, Vol. **VII** (SPIE) 2019, p. 11110.
[17] Phuoc K. T., Corde S., Thaury C., Malka V., Tafzi A., Goddet J. P., Shah R. C., Sebban S. and Rousse A., *Nat. Photon.*, **6** (2012) 308.
[18] Powers N. D., Ghebregziabher I., Golovin G., Liu C., Chen S., Banerjee S., Zhang J. and Umstadter D. P., *Nat. Photon.*, **8** (2014) 2831.
[19] Terzić B., Krafft G., Brown A., Hagerman T., Johnson E., Petrillo V., Drebot I., Maroli C. and Ruijter M., *EPL*, **126** (2019) 12003.
[20] Terzić B., Deitrick K., Hofler A. S. and Krafft G. A., *Phys. Rev. Lett.*, **112** (2014) 074801.
[21] Krafft G. A., *Phys. Rev. Lett.*, **92** (2004) 204802.
[22] Brau C. A., *Phys. Rev. ST Accel. Beams*, **7** (2004) 020701.
[23] Sakai Y. *et al.*, *Phys. Rev. Accel. Beams*, **20** (2017) 060701.
[24] Ghebregziabher I., Shadwick B. A. and Umstadter D., *Phys. Rev. ST Accel. Beams*, **16** (2013) 030705; see also arXiv:1204.1068.
[25] Heinzl T., Seipt D. and Kämpfer B., *Phys. Rev. A*, **81** (2010) 022125.
[26] Rykovanov S. G., Geddes C. G. R., Schroeder C. B., Esarey E. and Leemans W. P., *Phys. Rev. Accel. Beams*, **19** (2016) 030701.
[27] Seipt D., Rykovanov S. G., Surzhykov A. and Fritzsche S., *Phys. Rev. A*, **91** (2015) 033402.
[28] Terzić B. and Krafft G. A., *Phys. Rev. Accel. Beams*, **19** (2016) 098001.
[29] Ruijter M., Kharin V. Y. and Rykovanov S. G., *J. Phys. B: At., Mol. Opt. Phys.*, **51** (2018) 225701.
[30] Terzić B., Reeves C. and Krafft G., *Phys. Rev. Accel. Beams*, **19** (2016) 044403.
[31] Maroli C., Petrillo V., Drebot I., Serafini L., Terzić B. and Krafft G. A., *J. Appl. Phys.*, **124** (2018) 063105.

[32] KRAFFT G., JOHNSON E., DEITRICK K., TERZIĆ B., KELMAR R., HODGES T., MELNITCHOUK W. and DELAYEN J. R., *Phys. Rev. Accel. Beams*, **19** (2016) 121302.

[33] KRÄMER J. M., JOCHMANN A., BUDDE M., BUSSMANN M., COUPERUS J. P., COWAN T. E., DEBUS A., KÖHLER A., KUNTZSCH M., LASO GARCÍA A., LEHNERT U., MICHEL P., PAUSCH R., ZARINI O., SCHRAMM U. and IRMAN A., *Sci. Rep.*, **8** (2018) 1398.

[34] SUN C., LI J., RUSEV G., TONCHEV A. P. and WU Y. K., *Phys. Rev. Accel. Beams*, **12** (2009) 062801.

[35] CURATOLO C., DREBOT I., PETRILLO V. and SERAFINI L., *Phys. Rev. Accel. Beams*, **20** (2017) 080701.

[36] RANJAN N., TERZIĆ B., KRAFFT G., PETRILLO V., DREBOT I. and SERAFINI L., *Phys. Rev. Accel. Beams*, **21** (2018) 030701.

[37] FURMAN M., in *Conference Record of the 1991 IEEE Particle Accelerator Conference*, Vol. **1** (IEEE) p. 442.